

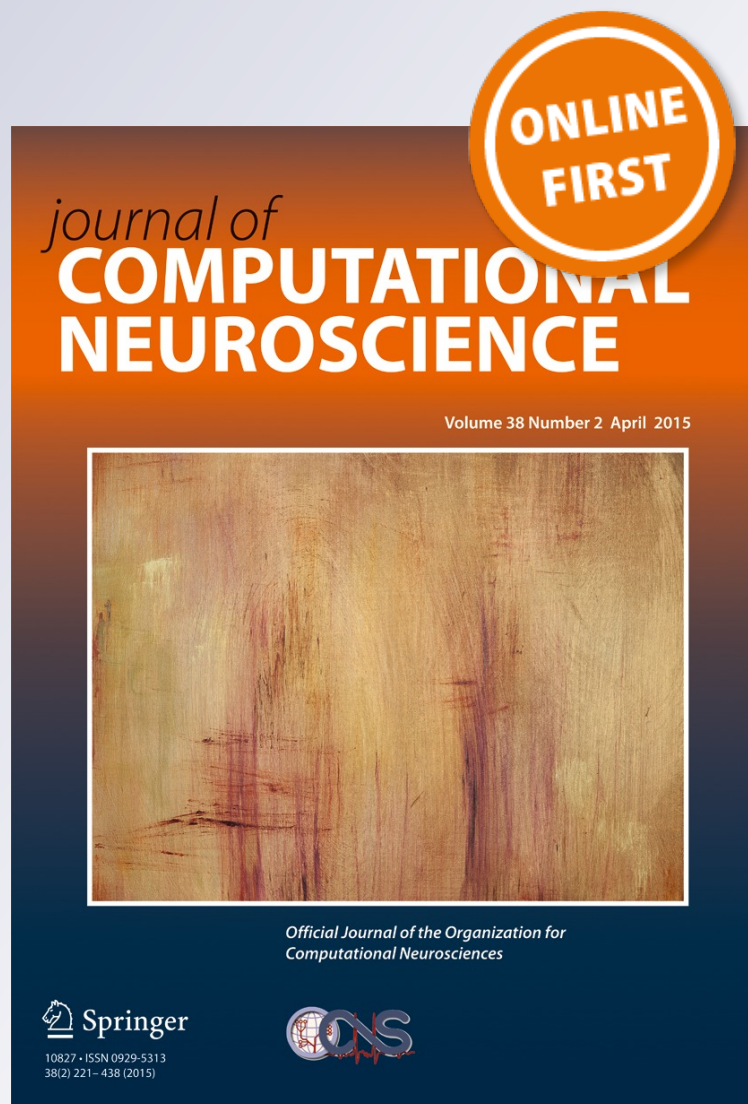
Interspike interval correlation in a stochastic exponential integrate-and-fire model with subthreshold and spike-triggered adaptation

LieJune Shiau, Tilo Schwalger & Benjamin Lindner

Journal of Computational Neuroscience

ISSN 0929-5313

J Comput Neurosci
DOI 10.1007/s10827-015-0558-4



Your article is protected by copyright and all rights are held exclusively by Springer Science +Business Media New York. This e-offprint is for personal use only and shall not be self-archived in electronic repositories. If you wish to self-archive your article, please use the accepted manuscript version for posting on your own website. You may further deposit the accepted manuscript version in any repository, provided it is only made publicly available 12 months after official publication or later and provided acknowledgement is given to the original source of publication and a link is inserted to the published article on Springer's website. The link must be accompanied by the following text: "The final publication is available at link.springer.com".

Interspike interval correlation in a stochastic exponential integrate-and-fire model with subthreshold and spike-triggered adaptation

LieJune Shiau¹ · Tilo Schwalger² · Benjamin Lindner^{3,4}

Received: 1 August 2014 / Revised: 11 February 2015 / Accepted: 20 March 2015
© Springer Science+Business Media New York 2015

Abstract We study the spike statistics of an adaptive exponential integrate-and-fire neuron stimulated by white Gaussian current noise. We derive analytical approximations for the coefficient of variation and the serial correlation coefficient of the interspike interval (ISI) assuming that the neuron operates in the mean-driven tonic firing regime and that the stochastic input is weak. Our result for the serial correlation coefficient has the form of a geometric sequence and is confirmed by the comparison to numerical simulations. The theory predicts various patterns of interval correlations (positive or negative at lag one, monotonically decreasing or oscillating) depending on the strength of the spike-triggered and subthreshold components of the adaptation current. In particular, for pure subthreshold adaptation we find strong positive ISI correlations that are usually ascribed to positive correlations in the input current. Our results i) provide an alternative explanation for interspike-interval correlations observed *in vivo*, ii) may be useful in fitting

point neuron models to experimental data, and iii) may be instrumental in exploring the role of adaptation currents for signal detection and signal transmission in single neurons.

Keywords Stochastic activity · Models of spiking neuron · Models of spike-frequency adaptation · Integrate-and-fire model · Interspike-interval correlations

1 Introduction

Neurons transmit and process information by sequences of action potentials (spikes) (Bear et al. 2007; Dayan and Abbott 2001). Spike generation appears often to be well described in a stochastic framework because the neural firing is affected by intrinsic noise source, as, for instance, channel noise (White et al. 2000) and by the massive synaptic input from many other (only weakly correlated) neurons (Destexhe et al. 2003). An important task of computational neuroscience is to identify the way that information about stimuli is encoded in the neural spike train (Rieke et al. 1996). A nontrivial step on this way is to understand the firing statistics first, i.e. to study which spike patterns are possible in the absence or presence of a sensory stimuli and which patterns can be expected due to the aforementioned intrinsic noise or the synaptic background.

One key feature of the firing statistics are correlations among the interspike intervals (ISI) of the spike train. Experimental evidence shows that ISIs are typically correlated over a few lags (Lowen and Teich 1992; Nawrot et al. 2007; Neiman and Russell 2001; Ratnam and Nelson 2000; Engel et al. 2008), and these correlations can have a strong effect on the neural information transmission (Ratnam and Nelson 2000; Chacron et al. 2001; Chacron et al. 2004; Avila-Akerberg and Chacron 2011). A number of mechanisms are known for inducing ISI correlations, such as

Action Editor: Nicolas Brunel

✉ Benjamin Lindner
benjamin.lindner@physik.hu-berlin.de

¹ Department of Mathematics, University of Houston, Houston TX 77058, USA

² Brain Mind Institute, École Polytechnique Fédérale de Lausanne (EPFL) Station 15, 1015 Lausanne, Switzerland

³ Bernstein Center for Computational Neuroscience Berlin, Philippstr. 13, Haus 2, 10115, Berlin, Germany

⁴ Department of Physics, Humboldt University Berlin, Newtonstr. 15, 12489, Berlin, Germany

correlated stimuli (so-called colored noise) (Middleton et al. 2003; Lindner 2004), or intrinsic noise from ion channels with slow kinetics (Fisch et al. 2012). Another prevalent mechanism for ISI correlations are the slow feedback processes mediating spike-frequency adaptation (Treves 1993; Chacron et al. 2000; Liu and Wang 2001; Benda et al. 2005), a phenomenon describing the reduced neuronal response to slowly changing stimuli (Benda and Herz 2003; Gabbiani and Krapp 2006). More specifically, the negative feedback from both subthreshold and spike-triggered adaptations impact the timing of neuronal spiking (Benda and Herz 2003; Benda et al. 2010; Gabbiani and Krapp 2006; Ladenbauer et al. 2012; Schwalger and Lindner 2013). The correlations of adapting neurons can show qualitatively different patterns, ranging from monotonically decaying to damped oscillatory correlations (Chacron et al. 2004; Chacron et al. 2001; Ratnam and Nelson 2000; Schwalger et al. 2010). Two of us have recently put forward a simple theory for ISI correlations of integrate-and-fire (IF) neurons with pure spike-triggered adaptation (Schwalger and Lindner 2013) that allowed us to relate features of the neural dynamics to various correlation patterns. However, the model in this study did not include subthreshold adaptation, that is relevant for many adaptation currents. How subthreshold adaptation affects ISI correlations is still poorly understood from the theoretical point of view and it is the central question of our study.

In this article, we study the popular two-dimensional adaptive exponential integrate-and-fire (aEIF) model, proposed by Brette and Gerstner (2005) as a combination of the exponential integrate-and-fire (EIF) model (Fourcaud-Trocmé et al. 2003) and a second slow variable as in Izhikevich's model (Izhikevich 2003). Besides the often studied form of spike-triggered adaptation, the system is also equipped with a subthreshold coupling between adaptation variable and voltage, which endows the model with much richer dynamical behavior and enables complex spiking patterns as worked out in detail by Touboul and Brette (2008) (it shares this rich repertoire of firing patterns with the earlier model by Izhikevich (2003)). We consider a stochastic version of the model that includes a white Gaussian current noise, mimicking in a simple way the fluctuations mentioned above. The advantages of the aEIF model - as opposed to other two-dimensional models of similar complexity - are the exponential spike initiation similar to that seen in real action potentials and a direct relation of its parameters to physiological ones. Moreover, the deterministic aEIF model exhibits a wide range of firing patterns (Clopath et al. 2007) that can be tuned to reproduce the behavior of all major classes of neurons. Remarkably, it has been successfully fit to Hodgkin-Huxley-type neurons (Brette and Gerstner 2005) as well as to recordings from cortical neurons (Jolivet et al. 2008).

We derive an analytical expression for the serial correlation coefficient (SCC) and the coefficient of variation (CV) in the mean-driven regime and under the assumption of weak noise. This expression is based on the characteristics of the deterministic aEIF model such as its phase response curve (PRC) and its Green's functions. We demonstrate that this theory correctly predicts the correlation pattern and coefficient of variation up to CVs of 0.2. Furthermore, we show that a weak and slow subthreshold adaptation has a weak effect on the correlation pattern. Most importantly, we show that strong pure subthreshold adaptation in the aEIF model results in positive correlations, that decay monotonically with the lag. This is in marked contrast to the pronounced negative correlations between adjacent ISIs, that have been so far regarded as the main effect of adaptation currents in stochastic neuron models.

Our paper is organized as follows. In the methods section, we introduce the model and statistics that are used in the paper and discuss the dynamical behavior of the model for strong mean input current. We then sketch the derivation of our main results. Theoretical predictions for the CV and SCC are compared to simulations of the models at different levels of noise and for the cases of pure subthreshold adaptation and spike-triggered adaptation, respectively. Furthermore, we inspect how the interspike interval correlations change upon varying the constant input current or the adaptation time scale. We conclude by a discussion of our findings in the biological context of neural signal transmission. Details of the deterministic dynamics (phase response curves, Green's functions) can be found in the Appendix.

2 Methods

2.1 Neuron model

We consider the adaptive exponential integrate-and-fire (aEIF) neuron model (Brette and Gerstner 2005; Touboul and Brette 2008) in a normalized setup similar to that studied in Schwalger and Lindner (2013)

$$\dot{v} = f(v) + \mu - a + \xi(t), \quad (1)$$

$$\tau_a \dot{a} = -a + Av + \tau_a \Delta \sum_i \delta(t - t_i), \quad (2)$$

Here time is measured in multiples of the membrane time constant. Equation (1) describes the evolution of the membrane equation, which is determined by the constant mean input current μ , a white noise current of vanishing mean value and correlation function $\langle \xi(t)\xi(t') \rangle = 2D\delta(t - t')$ ($\delta(t)$ is the Dirac delta function and D is the noise intensity). The nonlinear function

$$f(v) = -v + \Delta_T \exp[(v - 1)/\Delta_T]. \quad (3)$$

includes a leak term and an exponential function (approximating a persistent sodium current) with Δ_T being the slope factor quantifying the sharpness of the spike. Our choice of a vanishing leak reversal potential means that our voltage variable measures the difference to the leak reversal potential and that it is measured in multiples of the difference between leak reversal and the voltage at which the exponent of the exponential function switches its sign. As usual for integrate-and-fire models, upon reaching the threshold $v_{th} = 1.5$, we register a spike time t_i and reset the voltage to $v_r = 0$. For the remaining parameters of the voltage equation we choose $\mu = 25$, $\Delta_T = 0.2$, and $\tau_a = 5$.

The variable $a \geq 0$ enters Eq. (1) as a cell-intrinsic (non-synaptic) hyperpolarizing current and is governed by Eq. (2). The dynamics of a is affected by the voltage in two ways. First, the spikes generated by the aforementioned threshold criterion lead to an abrupt increase by Δ of the adaptation variable, the so-called *spike-triggered adaptation* corresponding to the last term on the r.h.s. in Eq. (2). Secondly, the subthreshold voltage v affects the adaptation variable also if no spike is generated. The strength of this *subthreshold adaptation* is quantified by parameter A . For simplicity, we adopt the assumption that the potential around which the subthreshold adaptation is linearized is equal to the leak potential (Brette and Gerstner 2005); any other value can be lumped into the base current by a simple transformation.

2.2 Behavior of the model with strong mean input current

In the absence of noise ($D = 0$), for sufficiently large input current μ and not too strong subthreshold adaptation, the aEIF neuron exhibits periodic spiking (Touboul and Brette 2008; Naud et al. 2008) (after transients due to initial conditions have decayed). In this case, there exists a deterministic limit cycle ($v_0(t), a_0(t)$) with a stable period T^* (i.e. ISI) and a constant value $a^* = a(t_i^+)$ (here $a(t_i^+)$ denotes the value immediately after the spike time t_i). Such a limit cycle for a large values of μ and A is shown in Fig. 1a. The figure also illustrates the existence of a fixed point, which is, however, unstable.

If we now increase the strength of subthreshold adaptation, the fixed point becomes stable via a subcritical Andronov-Hopf bifurcation. A typical trajectory for this case is shown in Fig. 1b and displays the bistability between the stable limit cycle (red) and the stable focus (blue). Both attractors are separated by an unstable limit cycle. For weak noise (e.g. $D=0.001$ as used in the simulation of Fig. 1) transitions between the two states do practically not occur in a finite simulation time. For larger noise, switchings between the two states may result in a high variability of the interspike interval. In the following, we will mark parameter

regions of bistability by a grey background in all plots where appropriate. For numerical simulations in this parameter regime we will always start the system close to the limit cycle (in the tonically firing state). Finally, if we go with the subthreshold adaptation parameter beyond a critical value (e.g. by choosing $A = 31.5$ as in Fig. 1c), the stable focus is the only remaining stable attractor¹ in the system (cf. Fig. 1c).

For our analytical approximation we will assume throughout the paper, that the system is kept close to the limit cycle and that noise is so weak that it changes the mean ISI, compared to the deterministic case, only little. We will see that our theory (which is entirely based on calculations of perturbations around the limit cycle) works well also in the region of bistability as long as we choose initial conditions close to the limit cycle.

2.3 Statistics of interest

Subsequent spike times of the model define the interspike intervals (ISIs) $T_i = t_i - t_{i-1}$. The firing rate of the neuron is given by the inverse of the mean interval

$$r = \frac{1}{\langle T_i \rangle} \tag{4}$$

where the average $\langle \dots \rangle$ is taken over the sequence of ISIs. It is instructive to relate time scales and rates in our non-dimensional model to real-time values. With a membrane time constant of $\tau_m = 20\text{ms}$, values of $\tau_a = 5$ and $r = 1$ correspond to an adaptation constant of 100ms and a firing rate of 50Hz.

The variability of the intervals can be quantified by the coefficient of variation (CV), the ratio of the intervals' standard deviation and its mean:

$$C_v = \frac{\sqrt{\langle (T_i - \langle T_i \rangle)^2 \rangle}}{\langle T_i \rangle} \tag{5}$$

The CV is zero for a strictly periodic spike train as, for instance, in our system generated in the absence of noise ($D = 0$). The CV of a completely random spike train, a Poisson process, is one.

The statistics of central interest in our study is the *serial correlation coefficient* (SCC), given by

$$\rho_k = \frac{\langle (T_i - \langle T_i \rangle)(T_{i+k} - \langle T_{i+k} \rangle) \rangle}{\langle (T_i - \langle T_i \rangle)^2 \rangle}, \tag{6}$$

where T_i and T_{i+k} are two ISIs, lagged by an integer k . A positive coefficient ρ_1 implies that adjacent intervals T_i and T_{i+1} show (on average) similar deviations from the mean,

¹In this case, the unstable subthreshold limit cycle still exists, while the unstable spike-associated limit cycle involving the voltage reset has become unstable itself. Perturbations around the spike limit cycle will grow in an oscillatory manner, can then overcome the inner unstable limit cycle due to the reset rule and go eventually to the stable focus.

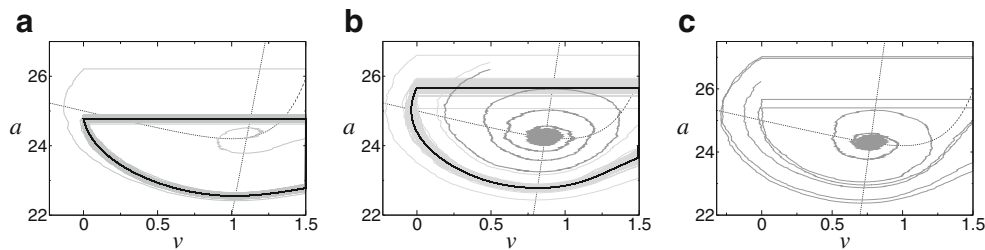


Fig. 1 Phase-space trajectories for different strength of subthreshold adaptation. **(a):** For a moderate value of $A = 22$ a stable limit cycle (thick solid line) is the only attractor in the system. Small noise ($D = 10^{-3}$ in all panels) will lead to small deviations from the limit cycle, that are described faithfully by our perturbation calculation. **(b):** For a larger value of $A = 28$, the stable limit cycle coexists with a stable fixed point (target of the thick dark grey trajectory). The fixed point is given by the intersection of the null clines (dotted lines in all panels) for the voltage, $a_{\dot{v}=0}(v) = f(v) + \mu$, and the adaptation variable, $a_{\dot{a}=0}(v) = Av$. The domain of attraction for the fixed point is rather

i.e. they are both shorter or both longer than $\langle T_i \rangle$. In contrast, negative correlations between adjacent intervals mean that a short interval is followed by a long one and/or vice versa. Typically, whatever the sign of the correlation is, they become smaller if we consider intervals that are further apart; in particular, $\lim_{k \rightarrow \infty} \rho_k = 0$.

We note that if the system operates in the bistable regime of coexistence of limit cycle and stable focus, our statistics is, strictly speaking, *not* stationary but conditioned on the initial values of v and a , which are chosen close to the stable limit cycle. The problem of the dwell times in either states and their effect on the ISI statistics is an interesting one but beyond the scope of this article.

2.4 Calculation of the SCC ρ_k

With weak noise input, both voltage $v(t)$ and adaptation variable $a(t)$ will deviate from the deterministic limit cycle, deviations that we denote by $\delta v(t) = v(t) - v_0(t)$ and $\delta a(t) = a(t) - a_0(t)$, respectively (here time t starts at a spike time t_i on the voltage reset). Obviously, also the roundtrip time is not fixed anymore but characterized by small deviations $\delta T_i = T_i - T^*$. While the voltage always starts with the same value, there is a variability in the starting points of $\delta a_i = \delta a(t_i^+) = a_i - a^*$. It is exactly this initial value in $a(t)$ that carries memory about previous ISIs and hence leads to correlations among the ISIs.

The weak deviation of the ISI, δT_{i+1} can be related to the perturbations by the noise and by the initial perturbation of the adaptation variable via the infinitesimal phase response curves (PRCs) of the system:

$$\delta T_{i+1} = - \int_0^{T^*} dt Z(t) \xi(t_i + t) - \delta a_i Z_a(0). \quad (7)$$

small: the light grey trajectory starts close to the initial point of the dark grey trajectory but ends up on the limit cycle. For long simulations started close to the limit cycle, the ISI statistics can still be described by our theory (which is based on perturbations around the limit cycle) because noise is too weak to observe any transitions to the fixed point attractor. **(c):** For $A = 31.5$ and, hence, beyond a critical value of A , the limit cycle solution is not stable anymore and only the stable fixed point exists. This excitable regime is clearly outside the scope of our analytical approximation. In all panels: $\Delta = 2, \mu = 25$

The PRCs $Z(t)$ and $Z_a(t)$ can be obtained through the *adjoint equations* of the linearized neuron model (see [Appendix](#)). In Eq. (7), the knowledge of $Z(t)$ suffices, because $Z_a(0) = - \int_0^{T^*} ds Z(s) e^{-s/\tau_a}$. We can rewrite the above equation as follows

$$\delta T_{i+1} = -Z_a(0) \delta a_i - \xi_i, \quad (8)$$

where $\xi_i = \int_0^{T^*} dt Z(t) \xi(t_i + t)$ is a sequence of uncorrelated Gaussian random numbers with correlation function

$$\langle \xi_i \xi_{i+k} \rangle = 2D \delta_{k,0} \int_0^{T^*} ds Z^2(t), \quad (9)$$

where $\delta_{i,j}$ is the Kronecker delta. A useful relation for the deviation δa_i is based on the formal integration of Eq. (2) over one ISI, connecting $a_{i+1} = a(t_{i+1}^+)$ and $a_i = a(t_i^+)$

$$a_{i+1} = a_i e^{-\frac{T_{i+1}}{\tau_a}} + \frac{A}{\tau_a} \int_{t_i}^{t_i+T_{i+1}} dt' v(t') e^{-\frac{(t_i-t')}{\tau_a}} e^{-\frac{T_{i+1}}{\tau_a}} + \Delta. \quad (10)$$

Without noise and under the assumption made above, this adaptation map (Touboul and Brette 2008) will approach a steady state, which is formally given by

$$a^* = \frac{\Delta + (A/\tau_a) e^{-T^*/\tau_a} \int_0^{T^*} ds v_0(s) e^{s/\tau_a}}{1 - \exp[-T^*/\tau_a]}. \quad (11)$$

This is not a closed-form solution, because it still contains the period T^* of the deterministic limit cycle and the voltage trajectory $v_0(t)$, which also depend on a^* .

In the presence of noise ($D > 0$), Eq. (10) can be linearized with respect to the small deviations $\delta v(t)$, δa_i , and δT_i results in

$$\delta a_{i+1} = \alpha \delta a_i - \beta \delta T_{i+1} + \alpha \frac{A}{\tau_a} \int_0^{T^*} ds \delta v(s) e^{s/\tau_a} \quad (12)$$

with

$$\alpha = \exp[-T^*/\tau_a], \tag{13}$$

$$\beta = a^* \frac{\alpha}{\tau_a} + A \frac{\alpha}{\tau_a} \left[\frac{1}{\tau_a} \int_0^{T^*} ds v_0(s) e^{s/\tau_a} - \frac{v_{th}}{\alpha} \right]. \tag{14}$$

Note that besides the obvious dependence on the amplitude A in these equations, the deterministic limit cycle $(v_0(t), a_0(t))$ and its period also depend on the strength of subthreshold and spike-triggered adaptation, A and Δ , respectively.

The last integral term in Eq. (12) can be expressed via the Green's function $\delta X_g(T^*, s)$ of the perturbation dynamics from Eqs. (1)-(2) (see Appendix), as

$$\frac{\alpha}{\tau_a} \int_0^{T^*} ds \delta v(s) e^{s/\tau_a} = -\delta a_i \int_0^{T^*} ds \delta X_g(T^*, s) e^{-s/\tau_a} + \int_0^{T^*} ds \delta X_g(T^*, s) \xi(t_i + s). \tag{15}$$

Combining this relation with Eq. (12) and Eq. (7), we obtain a stochastic map for δa_i :

$$\delta a_{i+1} = \alpha \theta \cdot \delta a_i + \eta_i \tag{16}$$

where

$$\theta = 1 + \frac{\beta Z_a(0)}{\alpha} - \frac{A}{\alpha} \int_0^{T^*} ds \delta X_g(T^*, s) e^{-s/\tau_a} \tag{17}$$

(where we used that $Z_a(0) = -\int_0^{T^*} ds \exp(-s/\tau_a) Z(s)$, see Appendix) and

$$\eta_i = \int_0^{T^*} ds (\beta Z(s) + A \delta X_g(T^*, s)) \xi(t_i + s) \tag{18}$$

are Gaussian random numbers with correlation function

$$\langle \eta_i \eta_{i+k} \rangle = 2D \delta_{k,0} \int_0^{T^*} ds (\beta Z(s) + A \delta X_g(T^*, s))^2 \tag{19}$$

The stochastic map Eq. (16) can be formally solved [by recursively applying Eq. (16)], yielding

$$\delta a_{i+k} = (\alpha \theta)^k \delta a_i + \sum_{j=0}^{k-1} (\alpha \theta)^j \eta_{i+k-1-j}, \tag{20}$$

from which by multiplication with δa_i and averaging, we obtain

$$\langle \delta a_{i+k} \delta a_i \rangle = (\alpha \theta)^k \langle \delta a_i^2 \rangle = (\alpha \theta)^k \frac{\langle \eta_i^2 \rangle}{1 - (\alpha \theta)^2} \tag{21}$$

(the last relation follows from squaring both sides of Eq. (16) and averaging).

We are ultimately interested in the correlations of the ISIs, which can be in the stationary case expressed according to Eq. (9) as

$$\langle \delta T_{i+k} \delta T_i \rangle = \langle \delta T_{i+k+1} \delta T_{i+1} \rangle = \langle (Z_a(0) \delta a_{i+k} + \xi_{i+k})(Z_a(0) \delta a_i + \xi_i) \rangle, \tag{22}$$

from which we get

$$\begin{aligned} \langle \delta T_{i+k} \delta T_i \rangle &= Z_a^2(0) (\alpha \theta)^k \frac{\langle \eta_i^2 \rangle}{1 - (\alpha \theta)^2} \\ &\quad + Z_a(0) (\alpha \theta)^{k-1} (1 - \delta_{k,0}) \langle \xi_i \eta_i \rangle \\ &\quad + 2D \delta_{k,0} \langle \xi_i^2 \rangle. \end{aligned} \tag{23}$$

From this relation, the variance of the ISI ($k = 0$) and the covariance can be determined and from these statistics we can calculate the CV and the SCC. Because the formulas are lengthy, a thoughtful choice of auxiliary expressions is helpful and convenient for checking limit cases.

For the squared CV we obtain

$$C_v^2 = \frac{2D}{(T^*)^2} \left(\bar{E} + \frac{\hat{\beta}}{1 - (\alpha \theta)^2} \bar{G} \right) \tag{24}$$

and for the SCC with $k > 0$ we get

$$\rho_k = \varphi^{k-1} \frac{(1 - \varphi^2) \hat{\beta} \bar{F} + \varphi \hat{\beta}^2 \bar{G}}{(1 - \varphi^2) \bar{E} + \hat{\beta}^2 \bar{G}}. \tag{25}$$

In these formulas we used the abbreviations:

$$\hat{\beta} = e^{-T^*/\tau_a} \frac{Z_a(0)}{\tau_a} \left[a^* + A \left(\int_0^{T^*} \frac{ds}{\tau_a} v_0(s) e^{s/\tau_a} - v_{th} e^{T^*/\tau_a} \right) \right], \tag{26}$$

$$\varphi = e^{-T^*/\tau_a} + \hat{\beta} - A \int_0^{T^*} ds e^{-s/\tau_a} \delta X_g(T^*, s), \tag{27}$$

$$\bar{E} = \int_0^{T^*} ds Z^2(s), \tag{28}$$

$$\bar{F} = \int_0^{T^*} ds Z(s) \left(Z(s) + \frac{A}{\hat{\beta}} Z_a(0) \delta X_g(T^*, s) \right), \tag{29}$$

$$\bar{G} = \int_0^{T^*} ds \left(Z(s) + \frac{A}{\hat{\beta}} Z_a(0) \delta X_g(T^*, s) \right)^2. \tag{30}$$

The values of T^* , a^* and $Z_a(0)$ and the functions $v_0(s)$, $Z(s)$, and $\delta X_g(s)$ can be determined numerically from the deterministic system; see Appendix.

In the limit case of $A = 0$ (pure spike-triggered adaptation), $\bar{E} = \bar{F} = \bar{G}$ and $\hat{\beta} = \varphi - e^{-T^*/\tau_a}$ (here Eq. (17) has been used). Using $\theta = \varphi/\alpha = \varphi e^{T^*/\tau_a}$, the SCC in this case reads

$$\rho_k = -(\alpha \theta)^{k-1} \frac{\alpha(1 - \theta)(1 - \alpha^2 \theta)}{1 + \alpha^2 - 2\alpha^2 \theta}, \tag{31}$$

which agrees with the result by Schwalger and Lindner (2013).

3 Results

Our general result for the SCC has the form

$$\rho_k = a \cdot b^{k-1}, k \geq 1. \quad (32)$$

Although the evaluation of the two parameters a and b requires numerical computations for the deterministic (noiseless) system, the result Eq. (32) allows already a number of insights without any numerical work.

First of all, the dependence of the serial correlation coefficient on the lag k is that of a geometric series. This is a remarkably simple result, which constrains possible SCC patterns, that can occur in this model. Compared to the previous result on pure spike-triggered adaptation (Schwalger and Lindner 2013), it also demonstrates that subthreshold adaptation does not change the principle mathematical structure of the solution. Secondly, the parameters a and b may attain different signs, which lead to different correlation patterns. For $b > 0$ the possible correlation patterns are a monotonic reduction of initially positive ($a > 0$) or negative ($a < 0$) correlations. For $b < 0$ the correlations oscillate with increasing lag, starting with a positive ($a > 0$) or negative ($a < 0$) correlation coefficient at lag one. As the numerical evaluation below reveals, in the presence of both subthreshold and spike-triggered adaptation, indeed all four correlations patterns can be found by varying parameters. Note that for the case of pure spike-triggered adaptation in an exponential integrate-and-fire neuron, only $b < 0$ is possible, corresponding to only two of the above four cases (Schwalger and Lindner 2013). Hence, although subthreshold adaptation does not change the geometric dependence on the lag, correlation patterns nevertheless change qualitatively under subthreshold adaptation because positive correlations become possible.

In the following we compare the theoretical results for the CV and the correlation coefficients to results of stochastic simulations of Eqs. (1) and (2). For completeness we will also compare the firing rate with its deterministic limit, i.e. the inverse of T^* , the limit cycle period of the noiseless system.

3.1 Possible correlation patterns

In Fig. 2 we compare the correlation coefficient ρ_k as a function of the lag to numerical simulations. We do so for various combinations of the subthreshold adaptation parameter A and the spike-triggered adaptation parameter Δ , including the cases of a pure subthreshold adaptation ($\Delta = 0$, first row in Fig. 2) and pure spike-triggered adaptation ($A = 0$, leftmost column in Fig. 2). All other parameters are fixed except for the noise intensity. We choose different noise intensities for different values of A (different columns in Fig. 2) because it is the small parameter of our theory.

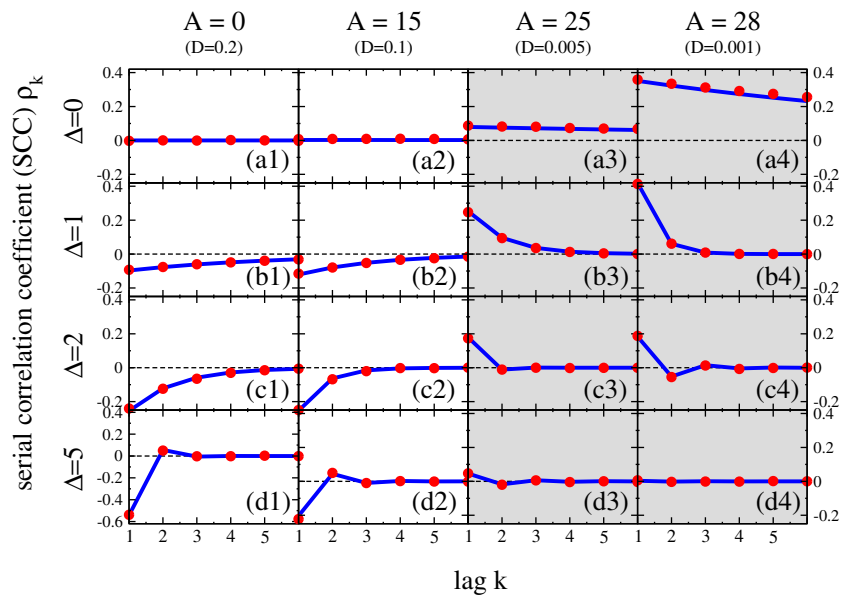
How small this parameter must be, depends strongly on the other parameters². Note that with our choice of parameters we condone that the model is not for all combinations of A and Δ in the physiological regime. If adaptation is switched off (i.e. for $A = 0$, $\Delta = 0$) we observe firing rates $r > 10$, which, assuming $\tau_m = 20$ ms, correspond to rates in real time that are larger than 500Hz. More physiologically reasonable parameter changes will be discussed below.

The simple parameter variation in Fig. 2 illustrates several points we want to make. First of all, if the noise level is appropriately adjusted, our theory (lines) can reproduce the simulation results (symbols) for a wide range of parameter values for the subthreshold and spike-triggered adaptation. The result of our calculation for perturbations around the limit cycle are valid in the tonic firing regime (all panels in Fig. 2 with white background) but also in the case of bistability between focus point and limit cycle (panels in Fig. 2 with grey background) if trajectories are started close to the limit cycle. Generally, as a rule of thumb, our theory works well for CVs below 0.2.

Secondly, as hypothesized above we can observe all kinds of correlation patterns that are possible according to Eq. (32). Starting with the trivial case of the renewal process in Fig. 2-a1 in absence of both adaptation mechanisms ($A = 0$, $\Delta = 0$), we see in the leftmost column the patterns for pure spike-triggered adaptation (Schwalger and Lindner 2013): a negative SCC at lag one that decays monotonically for small Δ , (e.g. Fig. 2-c1) or in an oscillatory fashion for larger values of Δ (c.f. Fig. 2-d1). For pure subthreshold adaptation ($\Delta = 0$, first row in Fig. 2), the neuron displays *positive* correlations at all lags. This is in marked contrast to the negative correlations induced by spike-triggered adaptation. Positive correlations can be as strong as $\rho_1 = 0.4$ for larger values of A (Fig. 2-a4). Positive correlations can be even enhanced if weak spike-triggered adaptation is added (compare e.g. Fig. 2-a3 and b3). By a combination of both spike-triggered and subthreshold adaptation, we can furthermore observe oscillatory correlations that start with $\rho_1 > 0$ (c.f. Fig. 2-c4). Finally, if both spike-triggered and subthreshold adaptation are very strong, serial correlations are suppressed (c.f. Fig. 2-d4). This can be explained as follows. Due to a strongly reduced firing rate, the adaptation process becomes fast compared to each single ISI — a limit, in which we can expect the spike statistics of a renewal process.

²Choosing a very small noise intensity for all parameters entails other difficulties: if the jitter of the interspike interval (order of $CV \cdot T^*$) becomes very small (of the order of the discrete time step Δt), numerical errors in the simulation results due to the discrete nature of our integration scheme can be expected. These errors can be reduced by decreasing the time step, which may become computationally expensive.

Fig. 2 Correlation patterns induced by spike-triggered and subthreshold adaptation. Comparison of theory (lines) and simulation results (symbols). Varied are the values of Δ (different rows) and A (different columns). For the different columns the value of the noise intensity has been adjusted as indicated. The grey shading indicates bistability of the deterministic system, i.e. for these parameters a stable focus point and the limit cycle coexist. Only perturbations of the limit cycle, however, are taken into account by our theory and play a role at the small noise intensities used in the simulations



Although positive correlations in our examples occur if the limit cycle coexists with the stable fixed point (as indicated by the grey background of the plots and as illustrated in Fig. 1b), such bistability is *not* a necessary condition for positive ISI correlations. Below we give a counter example.

In order to illustrate the interval statistics, we show in Fig. 3 time courses of the voltage and the adaptation variable and also plot the interspike interval sequence. We use two selected parameter sets from Fig. 2, namely, the case of strong pure spike-triggered adaptation (Fig. 2-d1) in (a) and that of strong subthreshold adaptation (Fig. 2-c3) in (b). In the former case, we observe a rather noisy voltage trace and an almost linear decay of the adaptation variable and we see explicitly how the ISIs deviate in an alternating fashion from the mean ISI. With a pronounced alternation, we can expect that adjacent intervals and intervals with an even number of intervals between them become negatively correlated and intervals with an odd number of intervals between them become positively correlated, i.e. we can expect a correlation coefficient that oscillates with the lag. For strong subthreshold adaptation with weaker noise shown in Fig. 3b, the voltage time series is more regular and the time course of the adaptation variable is nonmonotonic even for subthreshold voltage. This is due to the strong coupling between voltage and adaptation for large values of A and leads to pronounced positive correlations.

3.2 Effects of increasing the subthreshold adaptation on the firing statistics

Above we have verified that our theory leads to correct results, if the noise intensity is appropriately adjusted. Now, we are particularly interested in the effect of increasing

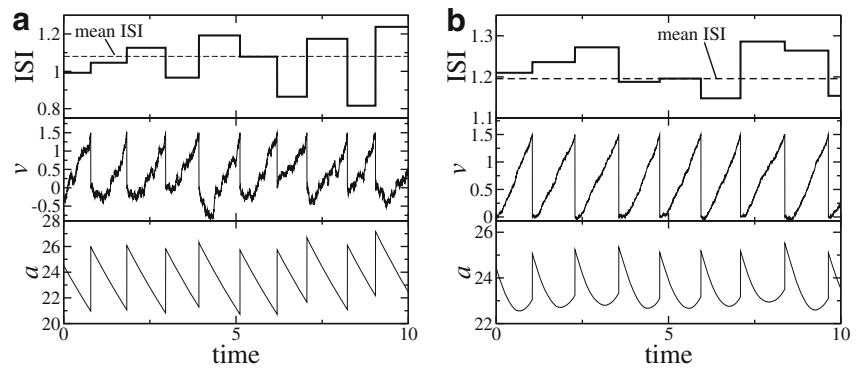
the subthreshold adaptation without changing any other parameters. We do this for two different values of the spike-triggered adaptation: $\Delta = 0$ in Fig. 4a to observe the way firing statistics changes in the case of pure subthreshold adaptation, and $\Delta = 5$ in Fig. 4b to observe the way subthreshold adaptation affects the correlation statistics with a pronounced spike-triggered adaptation. There is a natural limit for increasing A , because, as discussed above in Section 2.2, eventually the system will reach an excitable regime.

It becomes evident from Fig. 4a that a weak subthreshold adaptation alone ($\Delta = 0, A < 10$) affects the firing rate and the CV only little and does not cause strong ISI correlations. Larger values of A induce purely positive correlations and lead to a strong increase in the CV. The comparison with our theory reveals that values of the CV up to 0.2 are well reproduced by Eq. (24).

With finite spike-triggered adaptation ($\Delta = 5$ in Fig. 4b), there is a sizeable effect on the ISI correlations already at small values of A (below 10). The correlation coefficient at lag two, ρ_2 , for instance, increases by 40 % when we increase A from 0 to 10. Upon further increase of A both ρ_1 and ρ_2 change sign (as already discussed in the context of Fig. 2). The change takes place about $A = 20$, at which point the interval statistics may look like a renewal process. Interestingly, in the case of finite spike-triggered adaptation, the CV becomes a nonmonotonic function of the subthreshold adaptation strength; it displays a shallow minimum as a function of A .

The agreement of our theory with the simulation results is good at all inspected noise levels except if the system is deep in the bistable regime (shaded regions in Fig. 4), where finite noise may cause transitions between the limit cycle

Fig. 3 Time courses of membrane voltage and adaptation variable in two distinct cases with pronounced interspike interval correlations. SCC patterns become apparent by plotting the ISI sequence (solid line) and its mean value (dashed) versus time (top); voltage (middle) and adaptation variable (bottom) are shown as well. Parameters are as in Fig. 2-d1 (for panel a) and in Fig. 2-c3 (for panel b)



to the stable focus fixed point. Such bistability in the firing pattern will lead to strong variability of the ISI, which is reflected in large values of the CV. Because ISI correlations are solely due to perturbations of the tonic firing, the increased ISI variability will also lead to a reduction of the serial correlation coefficient (which is normalized by the ISI variance). This drop in ρ_k is indeed seen in all situations where the CV deviates strongly from the predictions of our limit-cycle-based theory.

As mentioned above, the high mean input used in Figs. 2 and 4 allowed us to detect all possible ISI correlation patterns by adjusting only the strength of spike-triggered adaptation and subthreshold adaptation. However, the strong mean drive also leads for some combinations of Δ and A to unphysiological values of the firing rate. In Fig. 5 we adjust the input current μ for every value of A such that we keep the firing rate at $r = 0.6$ (with $\tau_m = 20\text{ms}$ this corresponds to a physiologically plausible 30Hz firing rate in real time). Note that the constraint of fixed firing rate also

influences the range of possible A values. We compare again our theory to numerical simulations for pure subthreshold adaptation, $\Delta = 0$, in Fig. 5a and for mixed spike-triggered and subthreshold adaptation, $\Delta = 5$, in Fig. 5b and find in both cases a good agreement, in particular, for low noise intensities. While with fixed firing rate, the CV varies only little with A , the correlation coefficients depend strongly on its choice. Generally, increasing A causes a shift towards positive ISI correlations for both values of Δ . Remarkably, in this scaling it becomes evident in Fig. 5a that purely positive ISI correlations can be also observed outside the bistable parameter range of A (shaded parameter range), i.e. in the tonic firing regime (regions with white background in Fig. 5) that our theory was originally designed for. Hence, positive ISI correlations as predicted by our theory do not hinge on the presence of a stable focus in the deterministic dynamics.

The simplest way in which the firing statistics can be changed experimentally is to inject a constant current and to

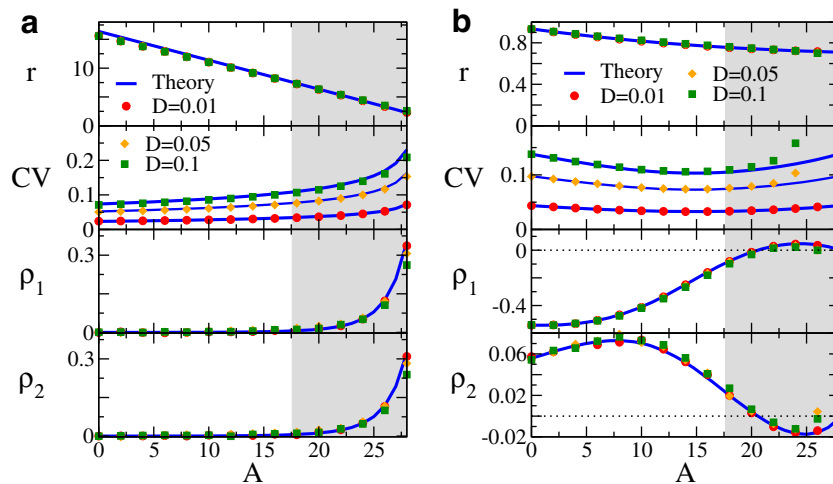


Fig. 4 Firing statistics as a function of strength of subthreshold adaptation. From top to bottom: firing rate, coefficient of variation of the interspike interval, serial correlation coefficient at lag one and at lag two. For all data we compare again theory (lines) to simulation results (symbols) obtained with fixed noise intensity as indicated. Note that in

our theory only the CV depends on the noise intensity (the other panels have only one theory curve). Strength of spike-triggered adaptation is $\Delta = 0$ in (a) [pure subthreshold adaptation] and $\Delta = 5$ in (b). The range of A for which the deterministic dynamics displays bistability between limit cycle and stable focus is marked in grey

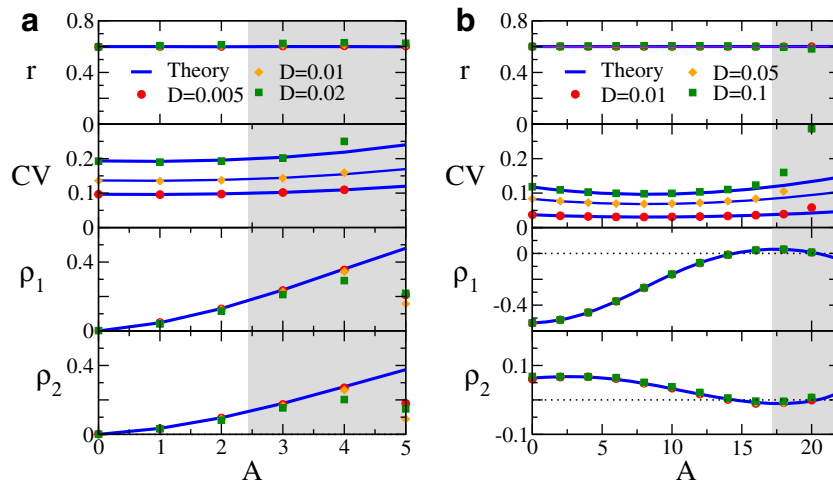


Fig. 5 Firing statistics as a function of strength of subthreshold adaptation with a fixed firing rate. From top to bottom: firing rate (kept at 0.6), coefficient of variation of the interspike interval, serial correlation coefficient at lag one and at lag two. For all data we compare again theory (*lines*) to simulation results (*symbols*) obtained with fixed noise intensity as indicated. Note that in our theory only the CV depends

vary its value. In our setup this corresponds to a variation of the parameter μ , illustrated in Fig. 6. Here we inspect two cases of weak (a) or moderate adaptation (b). In both cases, an increase in μ causes an increase in firing rate and a reduction of variability, which is in line with previous findings for white-noise driven integrate-and-fire neurons (Vilela and Lindner 2009). An increasing value of constant current leads to strong negative correlations between adjacent ISIs if A is small and Δ is large (Fig. 6a) and yields a transition from positive to negative correlations if the subthreshold component of adaptation is more pronounced (Fig. 6b). In particular, if the latter transition would be observed in a real neuron, this would suggest that both spike-triggered and subthreshold adaptation are present in this cell.

on the noise intensity (the other panels have only one theory curve). Strength of spike-triggered adaptation is $\Delta = 0$ in (a) [pure subthreshold adaptation] and $\Delta = 5$ in (b). The range of A for which the deterministic dynamics displays bistability between limit cycle and stable focus is marked in grey

Finally, we demonstrate in Fig. 7 that our theory works well for arbitrary values of the adaptation time constant τ_a by varying it over four orders of magnitude, i.e. our approach does not require a slow adaptation variable. First of all, ISI correlations vanish for $\tau_a \rightarrow 0$ because the adaptation variable decays too quickly to keep any memory about previous ISIs. In the opposite limit $\tau_a \rightarrow \infty$, correlations between adjacent intervals approach the value $-1/2$ while higher correlations decay again. On physical grounds the cumulative correlations $\sum_{j=1}^{\infty} \rho_j$ cannot become larger than $-1/2$ and, hence, adjacent intervals become perfectly anticorrelated if the adaptation time constant grows without bound. This is, however, also accompanied by a strong reduction of the firing rate.

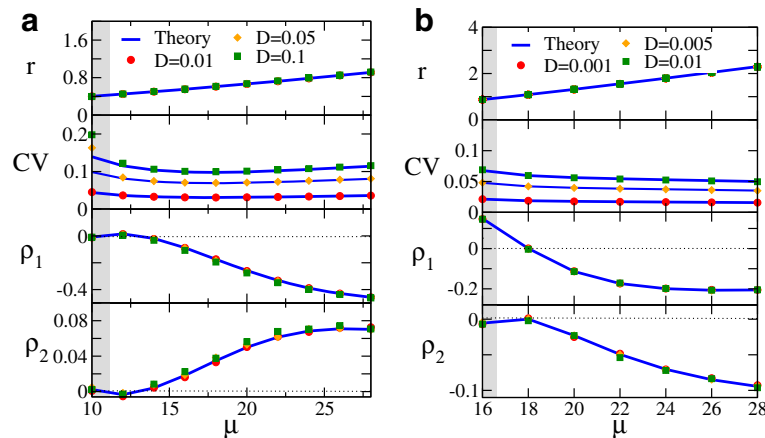


Fig. 6 Firing statistics as a function of input current. From top to bottom: firing rate, coefficient of variation of the interspike interval, serial correlation coefficient at lag one and at lag two. For all data we compare again theory (*lines*) to simulation results (*symbols*)

obtained with fixed noise intensity as indicated. Parameters are $A = 10$, $\Delta = 5$, $\tau_a = 5$, varying μ within $[10, 28]$ in (a), and Parameters are $A = 15$, $\Delta = 2$, $\tau_a = 3$, varying μ within $[16, 28]$ in (b), and all others remain the same

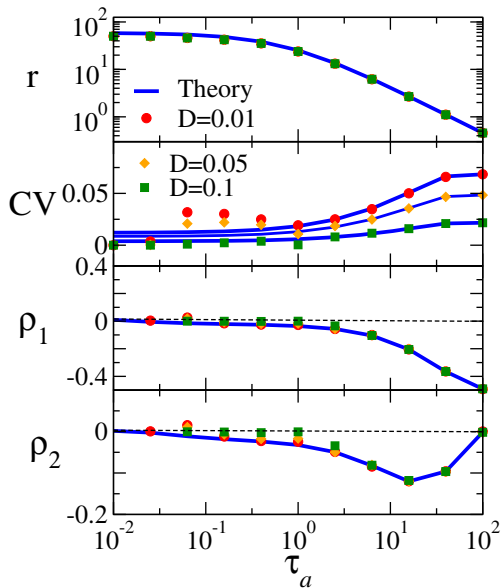


Fig. 7 Firing statistics as a function of the adaptation time constant. From top to bottom: firing rate, coefficient of variation of the interspike interval, serial correlation coefficient at lag one and at lag two. For all data we compare again theory (*lines*) to simulation results (*symbols*) obtained with fixed noise intensity as indicated. Remaining parameters are $A = 15$, $\Delta = 2$, $\mu = 100$

4 Summary and discussion

In this paper we have derived formulas for the CV and SCC of a white-noise driven exponential integrate-and-fire model with both spike-triggered and subthreshold adaptation. Our general result predicts a geometric dependence of the SCC on the lag. Furthermore, according to our theory by varying the adaptation parameters, we can achieve all possible correlation patterns with positive and negative correlations at lag one and a monotonic decay or a damped oscillation with respect to the lag. By comparison with extensive numerical simulations, we have demonstrated that our theory indeed reliably predicts all of these correlation patterns if the neuron is kept in the mean-driven tonic firing regime and if noise is weak. Moreover, our theory works as well in the regime of bistability (coexistence of a stable focus point and a stable limit cycle) if the model's initial condition is close to the tonic firing state and noise is sufficiently weak to avoid transitions to the stable fixed point.

Besides providing the general correlation structure, our theory relates the correlation statistics to properties of the deterministic neuron: its phase response curves with respect to perturbations in the voltage and in the adaptation current and the Green's function of the adaptation variable. These functions change in a complicated and intertwined manner when the adaptation parameters are changed. In particular, we can change the neuron from type I (for small or vanishing subthreshold adaptation) having a positive PRC at

all phases to type II (for strong subthreshold adaptation) having a PRC that is negative at early phases. These are the changes that also contribute to the qualitative change of the correlation pattern from negative ISI correlations for spike-triggered adaptation to positive ISI correlations for dominating subthreshold adaptation.

The results achieved in our paper may be useful in interpreting existing studies. Prescott and Sejnowski (2008) explored the role of subthreshold and spike-triggered adaptation for the signal transmission in conductance-based model neurons. These authors observed that only with spike-triggered adaptation strong negative ISI correlations are present, whereas for dominating subthreshold adaptation either only weak positive or vanishing ISI correlations are possible. Although they ascribed the positive correlations to the fact that a colored Ornstein-Uhlenbeck process was used as a stimulus of the model neuron, we have seen here that uncorrelated fluctuations combined with pure or dominating subthreshold adaptation can evoke positive ISI correlations.

Our results may be applied and extended in several directions. First of all, our theory provides a possible explanation for correlation patterns of spiking neurons *in vivo*. Importantly, the mechanism for nonrenewal spiking we have discussed here is a cellular mechanism (not a network mechanism) and thus should be present both *in vivo* as well as *in vitro*. Because so far positive ISI correlations have been mostly associated with correlations of the input, providing an alternative explanation based on cellular adaptation mechanisms is thus useful — although yet different mechanisms may exist that also lead to similar ISI correlations.

Secondly, our formulas for CV and SCC may be used as an additional tool for fitting parameters of the aEIF model to *in vivo* or *in vitro* data. White-noise stimuli are nowadays routinely applied to neurons *in vitro* and the resulting CV and ISI correlations can be useful as a mean to verify a parameter fit.

Thirdly, it is promising to apply our formulas to the analysis of the long-term variability of the count statistics. In fact, the CV and SCCs we have derived allow to compute the asymptotic limit of the spike count's Fano factor (Cox and Lewis 1966)

$$F_\infty = \lim_{t \rightarrow \infty} \frac{\langle \Delta N^2(t) \rangle}{\langle N(t) \rangle} = C_v^2 \left[1 + 2 \sum_{k=1}^{\infty} \rho_k \right]. \tag{33}$$

According to this formula, positive ISI correlations lead to an increase in the Fano factor, whereas negative correlations may strongly reduce it. Consequently, the detection of a static stimulus (based on estimates of spike counts) can be facilitated by negative correlations and will be deteriorated by positive ISI correlations. These effects are well-known

from numerical simulations (Chacron et al. 2001; Ratnam and Nelson 2000; Prescott and Sejnowski 2008) and simplified models (Chacron et al. 2004; Nikitin et al. 2012). In the framework of our theory, the effect of ISI correlations on signal detection can be inspected and discussed for a biophysically reasonable point neuron model.

Acknowledgments LS would like to thank the hospitality of Bernstein Center for Computational Neuroscience (BCCN) Berlin. LS was supported in part by the BCCN Berlin and by the National Science Foundation (DMS-1226282). TS and BL were supported by the Bundesministerium für Bildung und Forschung (FKZ:01GQ1001A). TS was supported by the European Research Council (Grant Agreement no. 268689, MultiRules).

Conflict of interests The authors declare that they have no conflict of interest.

Appendix

Phase response curves (PRC)

The phase-dependent sensitivity of the ISI in response to a stimulus $\epsilon\delta(t - t')$ added on the right-hand-side of Eq. (1) can be characterized by the infinitesimal PRC defined as

$$Z(t') = - \lim_{\epsilon \rightarrow 0} \frac{\delta T(t', \epsilon)}{\epsilon}$$

with $\delta T(t', \epsilon)$ being the change of the spike period due the δ -stimulation at the “phase” $t' \in [0, T^*]$. Analogously, the sensitivity with respect to a perturbation $\epsilon\tau_a\delta(t - t')$ added on the right-hand-side of Eq. (2) can be likewise defined by the negative infinitesimal relative change of the ISI. This sensitivity with respect to the adaptation variable will be denoted by $Z_a(t')$. Let the linearized system (1-2) be $\dot{X} = J(t)X$, and $X = (v, a)^T$ and $J(t)$ being the Jacobian matrix evaluated at the deterministic limit cycle $(v_0(t), a_0(t))^T$, then the infinitesimal PRCs $Z(t)$ and $Z_a(t)$ satisfy the *adjoint equations* $\dot{Y} = -J^T Y$ with $Y = (Z, Z_a)^T$ (Ermentrout and Terman 2010) as

$$\begin{pmatrix} \dot{Z} \\ \dot{Z}_a \end{pmatrix} = \begin{pmatrix} -\frac{\partial f(v_0, a_0)}{\partial v} & -\frac{A}{\tau_a} \\ 1 & \frac{1}{\tau_a} \end{pmatrix} \begin{pmatrix} Z \\ Z_a \end{pmatrix} \quad (34)$$

with the normalization condition $\dot{v}_0(t)Z(t) + \dot{a}_0(t)Z_a(t) = 1$, which can be calculated directly. On the threshold, a perturbation does not change the phase implying $Z_a(T^*) = 0$ (Schwalger and Lindner 2013). With this condition, the second equation of Eq. (34) satisfying $\dot{Z}_a = Z + \frac{1}{\tau_a}Z_a$ leads to $Z_a(0) = -\int_0^{T^*} Z(s)e^{\frac{-s}{\tau_a}} ds$.

Green's function

To calculate $\frac{A}{\tau_a} \int_0^{T^*} dt' \delta v(t') e^{-\frac{(T^*-t')}{\tau_a}}$, we start with the perturbation dynamics

$$\delta \dot{v} = \lambda(t)\delta v - \delta a + \xi(t), \quad (35)$$

$$\tau_a \delta \dot{a} = -\delta a + A\delta v, \quad (36)$$

where $\lambda(t) = df(v_0(t))/dv$, with initial conditions $\delta v(0) = 0, \delta a(0) = \delta a_i$. The solution to Eq. (36) is $\delta a(t) = \delta a_i e^{-t/\tau_a} + \delta x(t)$, where $\delta x(t)$ satisfies $\tau_a \delta \dot{x} = -\delta x + A\delta v$ with $\delta x(0) = 0$. Hence, the desired quantity is given by

$$\begin{aligned} & \frac{A}{\tau_a} \int_0^{T^*} \delta v(t') e^{-(T^*-t')/\tau_a} dt' = \delta x(T^*) \\ & = A \int_0^{T^*} dt' \delta X_g(T^*, t') [\xi(t') - \delta a_i e^{-t'/\tau_a}]. \end{aligned} \quad (37)$$

Here, we used the Green's function $\delta X_g(t, t')$ which is the solution of

$$\begin{aligned} \frac{\partial}{\partial t} \delta v_g(t, t') &= \lambda(t)\delta v_g(t, t') - A\delta X_g(t, t') + \delta(t-t'), \\ \tau_a \frac{\partial}{\partial t} \delta X_g(t, t') &= -\delta X_g(t, t') + \delta v_g(t, t'), \end{aligned} \quad (38)$$

with $\delta v_g(0, t') = \delta X_g(0, t') = 0$ and $t' \in [0, T^*]$. The two-dimensional system for the Greens function is solved numerically.

References

- Avila-Akerberg, O., & Chacron, M.J. (2011). Nonrenewal spike train statistics: causes and consequences on neural coding. *Experimental Brain Research*, 210, 353.
- Bear, M.F., Connors, B.W., & Paradiso, M.A. (2007). *Neuroscience: Exploring the brain*. Baltimore: Lippincott Williams and Wilkins.
- Benda, J., & Herz, A.V.M. (2003). A universal model for spike-frequency adaptation. *Neural Computation*, 15, 2523.
- Benda, J., Longtin, A., & Maler, L. (2005). Spike-frequency adaptation separates transient communication signals from background oscillations. *Journal of Neuroscience*, 25(9), 2312.
- Benda, J., Maler, L., & Longtin, A. (2010). Linear versus nonlinear signal transmission in neuron models with adaptation currents or dynamic thresholds. *Journal of Neurophysiology*, 104(5), 2806.
- Brette, R., & Gerstner, W. (2005). Adaptive Exponential Integrate-and-Fire model as an effective description of neuronal activity. *Journal of Neurophysiology*, 94(5), 3637.
- Chacron, M.J., Lindner, B., & Longtin, A. (2004). Noise shaping by interval correlations increases information transfer. *Physical Review Letters*, 92(8), 080601.
- Chacron, M.J., Longtin, A., & Maler, L. (2001). Negative interspike interval correlations increase the neuronal capacity for encoding time-dependent stimuli. *Journal of Neuroscience*, 21(14), 5328.
- Chacron, M.J., Longtin, A., St-Hilaire, M., & Maler, L. (2000). Suprathreshold stochastic firing dynamics with memory in p-type electroreceptors. *Physical Review Letters*, 85(7), 1576.

- Clopath, C., Jolivet, R., Rauch, A., Luscher, H., & Gerstner, W. (2007). Predicting neuronal activity with simple models of the threshold type: Adaptive Exponential Integrate-and-Fire model with two compartments. *Neurocomputing*, *70*(10-12), 1668.
- Cox, D.R., & Lewis, P.A.W. (1966). *The Statistical Analysis of Series of Events*. London: Chapman and Hall.
- Dayan, P., & Abbott, L.F. (2001). *Theoretical Neuroscience*. Cambridge: MIT Press.
- Destexhe, A., Rudolph, M., & Paré, D. (2003). The high-conductance state of neocortical neurons *in vivo*. *Nature Reviews Neuroscience*, *4*, 739.
- Engel, T.A., Schimansky-Geier, L., Herz, A.V.M., Schreiber, S., & Erchova, I. (2008). Subthreshold membrane-potential resonances shape spike-train patterns in the entorhinal cortex. *Journal of Neurophysiology*, *100*(3), 1576.
- Ermentrout, G.B., & Terman, D.H. (2010). *Mathematical Foundations of Neuroscience*. New York: Springer.
- Fisch, K., Schwalger, T., Lindner, B., Herz, A., & Benda, J. (2012). Channel noise from both slow adaptation currents and fast currents is required to explain spike-response variability in a sensory neuron. *Journal of Neuroscience*, *32*, 17332.
- Fourcaud-Trocmé, N., Hansel, D., van Vreeswijk, C., & Brunel, N. (2003). How spike generation mechanisms determine the neuronal response to fluctuating inputs. *Journal of Neuroscience*, *23*, 11628.
- Izhikevich, E. (2003). Simple model of spiking neurons. *IEEE Transactions Neural Networks*, *6*(14), 1569.
- Gabbiani, F., & Krapp, H.G. (2006). Spike-frequency adaptation and intrinsic properties of an identified, looming-sensitive neuron. *Journal of Neurophysiology*, *96*(6), 2951.
- Jolivet, R., Kobayashi, R., Rauch, A., Naud, R., Shinomoto, S., & Gerstner, W. (2008). A benchmark test for a quantitative assessment of simple neuron models. *Journal of Neuroscience Methods*, *169*, 417.
- Ladenbauer, J., Augustin, M., Shiao, L., & Obermayer, K. (2012). Impact of adaptation currents on synchronization of coupled exponential integrate-and-fire neurons. *PLoS Computational Biology*, *8*(4).
- Lindner, B. (2004). Interspike interval statistics of neurons driven by colored noise. *Physical Review E*, *69*(21).
- Liu, Y.H., & Wang, X.J. (2001). Spike-frequency adaptation of a generalized leaky integrate-and-fire model neuron. *Journal of Computational Neuroscience*, *10*(1), 25.
- Lowen, S.B., & Teich, M.C. (1992). Auditory-nerve action potentials form a nonrenewal point process over short as well as long time scales. *Journal of the Acoustical Society of America*, *92*, 803.
- Middleton, J.W., Chacron, M.J., Lindner, B., & Longtin, A. (2003). Firing statistics of a neuron model driven by long-range correlated noise. *Physical Review E*, *68*(21), 021920.
- Naud, R., Marcille, N., Clopath, C., & Gerstner, W. (2008). Firing patterns in the adaptive exponential integrate-and-fire model. *Biological Cybernetics*, *99*, 335.
- Nawrot, M.P., Boucsein, C., Rodriguez-Molina, V., Aertsen, A., Grün, S., & Rotter, S. (2007). Serial interval statistics of spontaneous activity in cortical neurons *in vivo* and *in vitro*. *Neurocomputing*, *70*(10-12), 1717.
- Neiman, A., & Russell, D.F. (2001). Stochastic biperiodic oscillations in the electroreceptors of paddlefish. *Physical Review Letters*, *86*(15), 3443.
- Nikitin, A., Stocks, N., & Bulsara, A. (2012). Enhancing the resolution of a sensor via negative correlation: a biologically inspired approach. *Physical Review Letters*, *109*, 238103.
- Prescott, S.A., & Sejnowski, T.J. (2008). Spike-rate coding and spike-time coding are affected oppositely by different adaptation mechanisms. *Journal of Neuroscience*, *28*, 13649.
- Ratnam, R., & Nelson, M.E. (2000). Nonrenewal statistics of electrosensory afferent spike trains: Implications for the detection of weak sensory signals. *Journal of Neuroscience*, *20*, 6672.
- Rieke, F., Warland, D., de Ruyter van Steveninck, R., & Bialek, W. (1996). *Spikes: Exploring the Neural Code*. Cambridge, Massachusetts: MIT Press.
- Schwalger, T., Fisch, K., Benda, J., & Lindner, B. (2010). How noisy adaptation of neurons shapes interspike interval histograms and correlations. *PLoS Computational Biology*, *6*, e1001026.
- Schwalger, T., & Lindner, B. (2013). Patterns of interval correlations in neural oscillators with adaptation. *Frontiers Computational Neuroscience*, *7*, 164.
- Touboul, J., & Brette, R. (2008). Dynamics and bifurcations of the adaptive exponential Integrate-and-Fire model. *Biological Cybernetics*, *99*(4-5), 319.
- Treves, A. (1993). Mean-field analysis of neuronal spike dynamics. *Network*, *4*(3), 259.
- Vilela, R.D., & Lindner, B. (2009). A comparative study of three different integrate-and-fire neurons: spontaneous activity, dynamical response, and stimulus-induced correlation. *Physical Review E*, *031909*, 80.
- White, J.A., Rubinstein, J.T., & Kay, A.R. (2000). Channel noise in neurons. *Trends in Neurosciences*, *23*(3), 131.